

On the possibility of p-type doping in barium stannate

Willis, Joe; Spooner, Kieran B.; Scanlon, David O.

DOI:

[10.1063/5.0170552](https://doi.org/10.1063/5.0170552)

License:

Creative Commons: Attribution (CC BY)

Document Version

Publisher's PDF, also known as Version of record

Citation for published version (Harvard):

Willis, J, Spooner, KB & Scanlon, DO 2023, 'On the possibility of p-type doping in barium stannate', *Applied Physics Letters*, vol. 123, no. 16, 162103. <https://doi.org/10.1063/5.0170552>

[Link to publication on Research at Birmingham portal](#)

General rights

Unless a licence is specified above, all rights (including copyright and moral rights) in this document are retained by the authors and/or the copyright holders. The express permission of the copyright holder must be obtained for any use of this material other than for purposes permitted by law.

- Users may freely distribute the URL that is used to identify this publication.
- Users may download and/or print one copy of the publication from the University of Birmingham research portal for the purpose of private study or non-commercial research.
- User may use extracts from the document in line with the concept of 'fair dealing' under the Copyright, Designs and Patents Act 1988 (?)
- Users may not further distribute the material nor use it for the purposes of commercial gain.

Where a licence is displayed above, please note the terms and conditions of the licence govern your use of this document.

When citing, please reference the published version.





Take down policy

While the University of Birmingham exercises care and attention in making items available there are rare occasions when an item has been uploaded in error or has been deemed to be commercially or otherwise sensitive.

If you believe that this is the case for this document, please contact UBIRA@lists.bham.ac.uk providing details and we will remove access to the work immediately and investigate.

RESEARCH ARTICLE | OCTOBER 19 2023

On the possibility of p-type doping in barium stannate

Joe Willis  ; Kieran B. Spooner  ; David O. Scanlon  

 Check for updates

Appl. Phys. Lett. 123, 162103 (2023)

<https://doi.org/10.1063/5.0170552>


View
Online


Export
Citation

CrossMark

Articles You May Be Interested In

Temperature and pressure dependent thermodynamic behavior of 2H-CuInO₂

AIP Conference Proceedings (May 2018)

Properties of transparent zinc-stannate conducting films prepared by radio frequency magnetron sputtering

J. Vac. Sci. Technol. A (May 1995)

Zinc stannate flakes for optoelectronic and antibacterial applications

AIP Conference Proceedings (July 2019)

starting at
EUR 6,360,-



Grows with your experiment. The MFLI Lock-in Amplifier.

Field-upgradeable options

- 5 MHz frequency extension
- Multi-frequency analysis
- PID controller
- Impedance analyzer



[Find out more](#)

On the possibility of p-type doping in barium stannate

Cite as: Appl. Phys. Lett. **123**, 162103 (2023); doi: [10.1063/5.0170552](https://doi.org/10.1063/5.0170552)

Submitted: 3 August 2023 · Accepted: 9 October 2023 ·

Published Online: 19 October 2023



View Online



Export Citation



CrossMark

Joe Willis,^{1,2}  Kieran B. Spooner,^{1,2,3}  and David O. Scanlon^{1,2,3,a)} 

AFFILIATIONS

¹Department of Chemistry, University College London, 20 Gordon Street, London WC1H 0AJ, United Kingdom

²Thomas Young Centre, University College London, Gower Street, London WC1E 6BT, United Kingdom

³School of Chemistry, University of Birmingham, Edgbaston, Birmingham B15 2TT, United Kingdom

^{a)} Author to whom correspondence should be addressed: d.o.scanlon@bham.ac.uk

ABSTRACT

The combination of optical transparency and bipolar dopability in a single material would revolutionize modern opto-electronics. Of the materials known to be both p- and n-type dopable (such as SnO and CuInO₂), none can satisfy the requirements for both p- and n-type transparent conducting applications. In the present work, perovskite BaSnO₃ is investigated as a candidate material: its n-type properties are well characterized, with La-doping yielding degenerate conductivity and record electron mobility, while it has been suggested on a handful of occasions to be p-type dopable. Herein, group 1 metals Li, Na, and K and group 13 metals Al, Ga, and In are assessed as p-type acceptor defects in BaSnO₃ using a hybrid density functional theory. It is found that while K and In can induce hole concentrations up to 10¹⁶ cm⁻³, the low energy oxygen vacancy pins the Fermi level in the bandgap and ultimately prevents metallic p-type conductivity being achieved in BaSnO₃. Nevertheless, the predicted hole concentrations exceed experimentally reported values for K-doped BaSnO₃, suggesting that the performance of a transparent p-n homo-junction made from this material could be significantly improved.

© 2023 Author(s). All article content, except where otherwise noted, is licensed under a Creative Commons Attribution (CC BY) license (<http://creativecommons.org/licenses/by/4.0/>). <https://doi.org/10.1063/5.0170552>

Materials that display the dual properties of optical transparency and metallic-like conductivity are sparse, but they are almost universally required in modern technologies:¹⁻³ as transparent contacts in solar cells;⁴ thin film transistors in display and touch-screen technology;^{5,6} and coatings in smart and low-emission windows.⁷ The transparent conducting materials (TCMs) used in the above applications are invariably n-type post-transition metal oxides (such as Sn-doped In₂O₃, F-doped SnO₂, and Al-doped ZnO), which routinely display electron conductivity on the order of 1000 to 10 000 S cm⁻¹, electron mobility on the order of 10 to 100 cm² V⁻¹ s⁻¹, and optical transmission above 90%.⁵ Meanwhile, the development of p-type TCMs has been less successful—hole conductivity and mobility are often 1 to 2 orders of magnitude lower, optical transparency is much harder to achieve, and the chemical and thermal stability of p-type TCMs is often poorer than the n-type metal oxides.^{2,3} This disparity between p- and n-type TCM technology is a major bottleneck in the development of the next generation of opto-electronic devices, which will have at their heart *fully transparent p-n junctions*.

The motivation for the present work is a 2016 publication by Kim *et al.*, entitled “Thermally stable p-n-junctions based on a single

transparent perovskite semiconductor BaSnO₃,⁸ where K-doped (p-type) and La-doped (n-type) BaSnO₃ were deposited via pulsed laser deposition (PLD) to fabricate a transparent p-n junction. Perovskite BaSnO₃ is well characterized as a TCM,⁹⁻¹² with an optical gap of around 3.6 eV, conductivity up to 5000 S cm⁻¹ when doped with La, and single crystal electron mobility up to 320 cm² V⁻¹ s⁻¹, which is the record for any transparent material. Its defect chemistry has been studied previously with hybrid density functional theory (DFT), indicating weak n-type semiconducting behavior when undoped, and degenerate conductivity when doped with La or F.¹³⁻¹⁶ However, computational investigation into its p-type defect chemistry have thus far been overlooked.

The combination of optical transparency and *bipolar* conductivity in a single material, implying the possibility of a transparent p-n *homo-junction*, is a lucrative prospect, as it would simplify deposition and minimize strain at the interface between the p- and n-type layers within a device (compared to a p-n *hetero-junction* such as SnO-SnO₂).¹⁷ Hole mobility on the order of 10 cm² V⁻¹ s⁻¹ would position BaSnO₃ as a competitive p-type transparent conductor, comparable with other p-type materials such as CuI and SnO, and would

push an all-BaSnO₃ device beyond simply proof-of-concept. Achieving bipolarity in BaSnO₃ is particularly appealing due to its perovskite structure, which could enable a transparent p–n homo-junction as part of a larger perovskite oxide device with relative ease. In this Letter, the basic crystal and electronic structure properties of BaSnO₃ are reported, and group 1 and group 13 cations are considered as p-type defects using hybrid DFT calculations. Charge transport properties are predicted at the carrier density suggested by the defect chemistry, and an upper theoretical limit to hole mobility is offered. The defect chemistry of BaSnO₃ is discussed in relation to the other post-transition metal TCMs and in the context of fabricating transparent p–n homo-junctions.

All DFT calculations were performed using VASP, a plane wave basis set code that uses projector augmented wave (PAW) pseudopotentials to describe the interactions between core and valence electrons.^{18–23} The PBE0 hybrid density functional was used for all relaxations and electronic structure calculations,²⁴ which has been shown to accurately predict electronic structure properties of Sn(IV) compounds in the literature,^{13,25} while the PBEsol functional was used for density functional perturbation theory (DFPT) calculations.²⁶ Spin–orbit coupling effects were not included, as they have been shown to be negligible in BaSnO₃.²⁷ The supercell method (containing 135 atoms) was used to simulate defects in BaSnO₃, and formation energies were calculated using the method proposed by Lany and Zunger.^{28,29} Charge transport properties were modeled using the AMSET code and plotted using the ThermoParser package.^{30,31} The py-sc-fermi package,³² based off the original Fortran SC-FERMI code,³³ was used to calculate the self-consistent Fermi level (SCFL) and defect concentrations and to plot the transition level diagrams, while the CPLAP software was used to calculate the chemical potential limits of BaSnO₃.³⁴ Crystal structures were visualized using the VESTA package,³⁵ and electronic structure plots were produced using the sumo

package.³⁶ Further computational details can be found in the supplementary material.

Basic crystal and electronic structure properties of BaSnO₃ are summarized in Fig. 1. It is a cubic perovskite, crystallizing in the $Pm\bar{3}m$ space group, and the calculated lattice parameter of 4.12 Å is in excellent agreement with both experimental (4.12 Å) and computational (4.13 Å) studies.^{9,13,37} The strong overlap of unoccupied Sn 5s states with O 2p anti-bonding states results in the highly dispersed conduction band minimum (CBM) that is characteristic of the n-type TCMs and is facilitated by the high-symmetry, corner-sharing SnO₆-octahedral network that is native to the perovskite structure. The near-perfect Goldschmidt tolerance factor (1.026)³⁸ in BaSnO₃ enables this strong interaction throughout the SnO₆ network and yields a parabolic electron effective mass of 0.25 m_e , indicative of the high electron mobility that is observed experimentally. Meanwhile, the O 2p dominated valence bands are flat in nature, typical of highly localized electronic states, with average parabolic hole effective masses of 0.84 m_e , 0.90 m_e , and 8.57 m_e . The indirect and direct gaps are 3.19 and 3.59 eV, respectively, and are in excellent agreement with previous computational studies.^{13,37}

To make p-type BaSnO₃, low energy p-type acceptor defects must be introduced close to the valence band maximum (VBM), while n-type donor defects must be minimized. Previous hybrid DFT calculations have identified the oxygen vacancy, V_O, as the lowest energy n-type species—this defect is recalculated in the present work (with excellent agreement in formation energy and transition level position) and is assumed to be the main charge compensation center.¹³ The group 1 metals Li, Na, and K (referred to as M^I), as well as the group 13 metals Al, Ga and In (referred to as M^{XIII}), are considered as candidate dopants, and the types of defect they can form are summarized as follows: M_{Ba}^I, M_{Sn}^I, and M_{Sn}^{XIII} substitutions can accept electrons from the VBM and act as p-type species; M_{Ba}^{XIII}, M_{int}^I, and M_{int}^{XIII} can donate

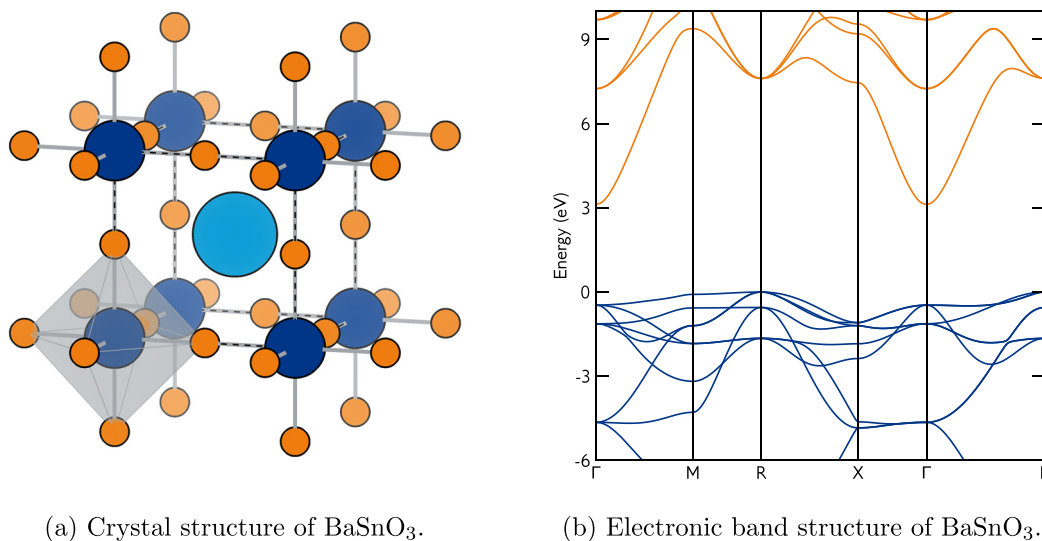
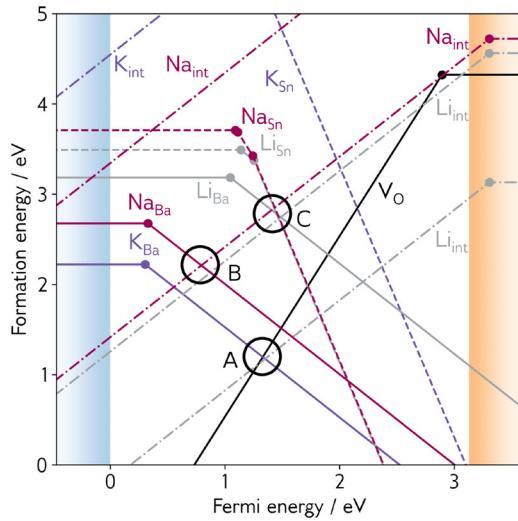
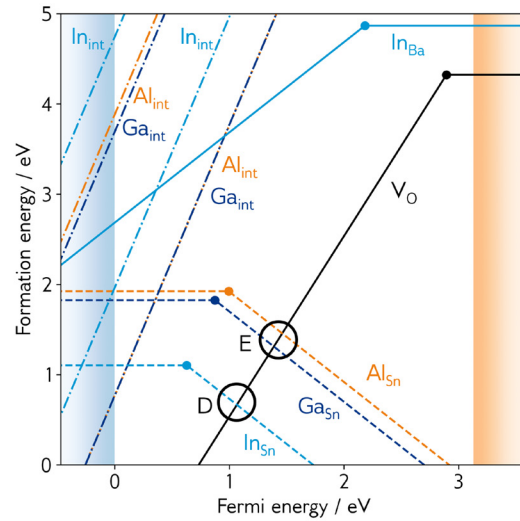


FIG. 1. (a) Conventional unit cell of $Pm\bar{3}m$ BaSnO₃, $a = 4.12$ Å; light blue, dark blue, and orange atoms denote Ba, Sn, and O, respectively; plotted using the VESTA software;³⁵ (b) Band structure of BaSnO₃; indirect gap ($R \rightarrow \Gamma$) 3.13 eV; direct gap ($\Gamma \rightarrow \Gamma$) 3.59 eV; parabolic electron effective mass 0.25 m_e ; parabolic hole effective mass 0.84 m_e , 0.90 m_e , and 8.57 m_e ; blue and orange lines denote valence and conduction bands, respectively; plotted using the sumo software.³⁶



(a) M^I doping: Li, Na and K are grey, magenta and lavender, respectively.



(b) M^{XIII} doping: Al, Ga and In are orange, dark blue and light blue, respectively.

FIG. 2. Transition level diagrams for (a) group 1 (M^I) and (b) group 13 (M^{XIII}) doped BaSnO_3 ; VBM and CBM denoted by blue and orange shaded areas, respectively; V_O denoted by solid black line; M_{Ba} , M_{Sn} , and M_{int} denoted by solid, dashed, and dotted-dashed lines, respectively; A, B, C, D, and E denote regions of interest and are explained in the main text.

electrons to the CBM and act as n-type species. The transition level diagrams for M^I and M^{XIII} doping under the most p-type growth conditions (metal poor, oxygen rich) are shown in Fig. 2, and a summary of Shannon ionic radii and Goldschmidt tolerance factors can be found in Table I.

Considering first the M^I dopants, it can be seen that the lowest energy p-type species is the K_{Ba} substitution, with a formation energy of just over 2 eV and a relatively shallow transition level around 300 meV from the VBM. However, as highlighted at point A in Fig. 2(a), the hole generated by the K_{Ba} defect is charge compensated by the electrons introduced by V_O , pinning the Fermi level in the bandgap. In fact, the oxygen vacancy is low enough in energy to charge compensate all the p-type M^I substitutions, severely compromising their ability to generate net p-type charge carriers in BaSnO_3 . The oxygen vacancy defect is discussed in greater detail in the supplementary material.

TABLE I. Tolerance factors for compositions in the dopant phase space; r Shannon ionic radius for each species;³⁹ coordination number VI for Al, Ga, In, Li; coordination numbers VI and XII available for Na, K.

Species	r (Å)	t_{ASnO_3}	t_{BaBO_3}
Ba^{2+}	1.61 ^{XII}	1.026 ^{XII}	...
Sn^{4+}	0.69 ^{VI}	...	1.026 ^{VI}
Li^{1+}	0.76 ^{VI}	0.731 ^{VI}	0.992 ^{VI}
Na^{1+}	1.02 ^{VI} ; 1.39 ^{XII}	0.950 ^{XII}	0.883 ^{VI}
K^{1+}	1.38 ^{VI} ; 1.64 ^{XII}	1.036 ^{XII}	0.767 ^{VI}
Al^{3+}	0.54 ^{VI}	0.653 ^{VI}	1.110 ^{VI}
Ga^{3+}	0.62 ^{VI}	0.683 ^{VI}	1.063 ^{VI}
In^{3+}	0.80 ^{VI}	0.745 ^{VI}	0.974 ^{VI}

The Na_{Ba} substitution is approximately 0.5 eV higher in energy than K_{Ba} , and undergoes self-compensation by Na_{int} species, as highlighted at point B; similarly, Li_{Ba} is self-compensated by Li_{int} at point C. This is observed for Na and Li because their ionic radii are reasonably small (1.02 and 0.76 Å compared to the 1.61 Å of Ba), greatly reducing the energy of the interstitial defect species and increasing the energy of the substitution species due to the size mismatch. In the case of K, the interstitial defect is several eV higher in energy (and the substitution lower) due to its larger ionic radius of 1.38 Å and, therefore, does not self-compensate. These thermodynamic preferences for Ba site substitution are reflected in the values for t_{ASnO_3} in Table I—the greater the deviation from a perfect t , the more significant the energy penalty. Substitution onto the Sn site is unlikely for all three dopants due to the prohibitively high formation energies, and in any case undergoes significant charge compensation from various interstitial species, as well as the oxygen vacancy.

A final point on the M^I species is the notable difference in the position of the $0 \rightarrow 1-$ transition level of Li_{Ba} compared to Na_{Ba} and K_{Ba} , occurring at a Fermi energy of around 1.0 eV rather than 0.3 eV. This is because the Li ionic radius is so small that the formation of a hole distorts the dopant off the traditional perovskite “A-site” to a square planar-like coordination, resulting in a trapped polaron [Fig. 3(a)]. This is in contrast to the larger Na and K species, which remain on the A-site, resulting in a more delocalized hole and a correspondingly shallower transition level [Fig. 3(b)]. It is noted that the defect potential energy surfaces of Na_{Ba} and K_{Ba} were thoroughly explored using the ShakeNBreak methodology (via the application of systematic bond length distortions around a defect site before relaxation),^{40,41} but the energy-lowering, symmetry-breaking distortion exhibited by Li_{Ba} was not reproduced.

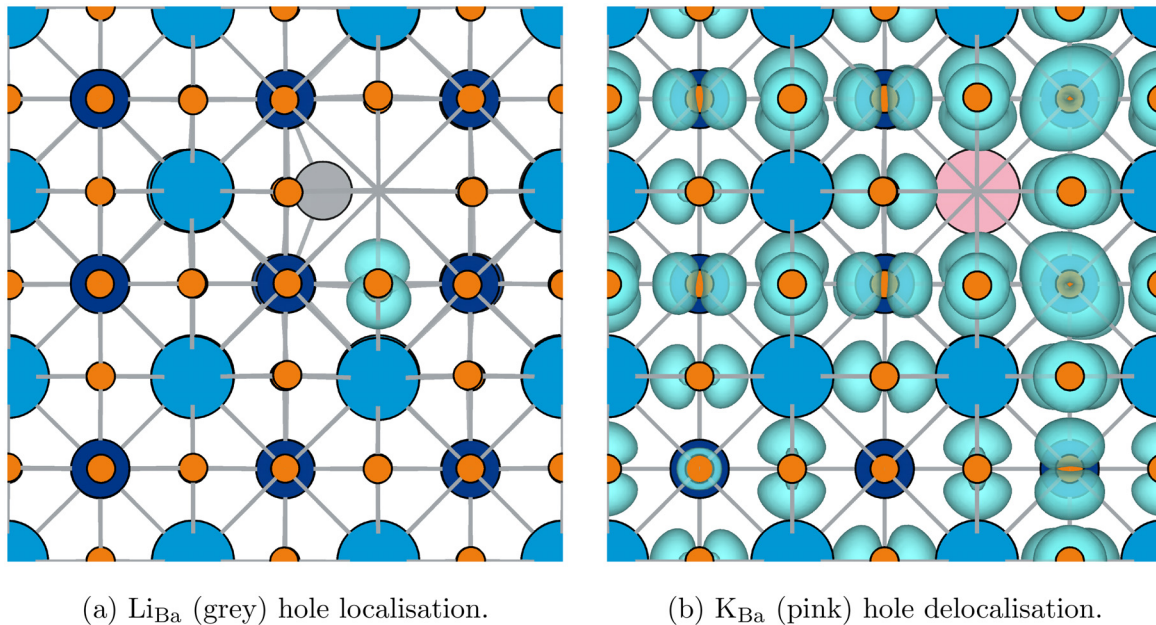


FIG. 3. Partial charge density of the hole (light blue) generated by Ba site substitution; light blue, dark blue, and orange atoms denote Ba, Sn, and O, respectively; plotted with an isosurface density of $0.06 \text{ e}\text{\AA}^{-3}$.

Turning now to the M^{XIII} dopants, In_{Sn} is clearly the best candidate with a formation energy just over 1 eV. The Al and Ga substitutions are around 0.8 eV higher in energy and show slightly deeper transition levels, indicative of increased structural distortion around the defect site. This is expected as the ionic radii of Al and Ga are significantly smaller than that of In (0.54, 0.62, and 0.80 Å, respectively, with Ga being smaller than expected due to the scandide contraction), and are less able to stabilize the MO_6 octahedron within the perovskite structure (refer to the t_{BaBO_3} tolerance factors in Table I). The transition levels of all three M^{XIII} substitutions are quite deep, resulting in trapped hole polarons (as shown for In_{Sn} in Fig. 4).

Analogous to the case of the M^{I} dopants, the oxygen vacancy is expected to charge compensate the holes generated by the p-type substitutions, as highlighted by points D and E in Fig. 2(b). However, self-compensation is not predicted to be an issue for the M^{XIII} species, due to the higher formation energies and charge states of the interstitial species, compared to the M^{I} series. Furthermore, n-type substitution onto the Ba site requires prohibitively high formation energies (nearly 5 eV for In_{Ba} and several eV higher for the remaining two), ruling out self-compensation from undesirable cation site substitution.

While an interesting test-bed for investigating ionic radii effects during doping, the results are hardly promising for achieving high performance p-type BaSnO_3 . In fact, calculation of defect concentrations, under the assumption of thermal equilibrium, and the position of the self-consistent Fermi level (SCFL, at a synthesis temperature of 1050 K as reported by Kim *et al.* in their PLD experiment)⁸ indicate that it should not be possible to achieve metallic-like p-type conductivity in BaSnO_3 , as shown in Table II. For K-doping, the SCFL is found at 1.38 eV, while for In-doping it drops down to 1.12 eV—the ideal position of the SCFL for a degenerate p-type semiconductor is within $k_B T$ of the VBM.

Despite the reasonably high concentration of p-type substitutional defects (particularly in the case of In-doping), hole carrier densities are limited to 5.2×10^{14} and $9.8 \times 10^{15} \text{ cm}^{-3}$ for K- and In-doping, respectively (equivalent to rather poor conductivities of 4.97×10^{-4} and $1.99 \times 10^{-3} \text{ Scm}^{-1}$). This is due to the low energy

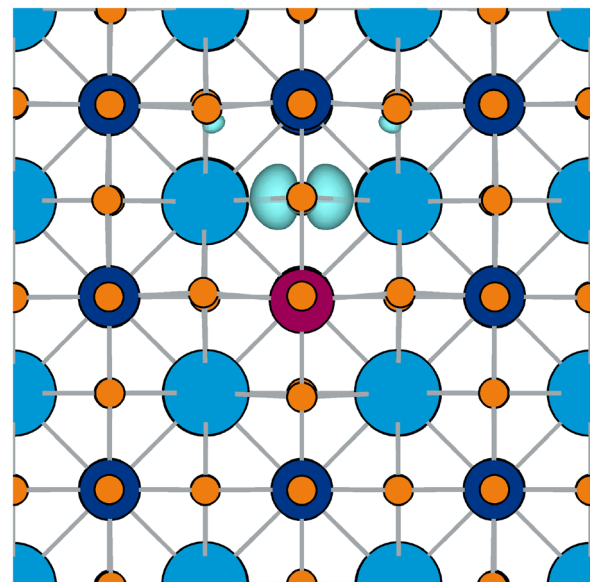


FIG. 4. Partial charge density of the hole (light blue) generated by In_{Sn} (magenta) substitution; light blue, dark blue, and orange atoms denote Ba, Sn, and O, respectively; plotted with an isosurface density of $0.01 \text{ e}\text{\AA}^{-3}$.

TABLE II. Predicted hole density and equilibrium defect concentrations of low energy species in BaSnO₃ at 1050 K, calculated using the py-sc-fermi package.³²

K-doping	$n_{1050\text{K}}$ (cm ⁻³)	In-doping	$n_{1050\text{K}}$ (cm ⁻³)
h^+	5.2×10^{14}	h^+	9.8×10^{15}
K_{Ba}^{1-}	4.7×10^{16}	$\text{In}_{\text{Sn}}^{1-}$	1.6×10^{19}
V_{O}^{2+}	2.3×10^{16}	V_{O}^{2+}	8.2×10^{18}

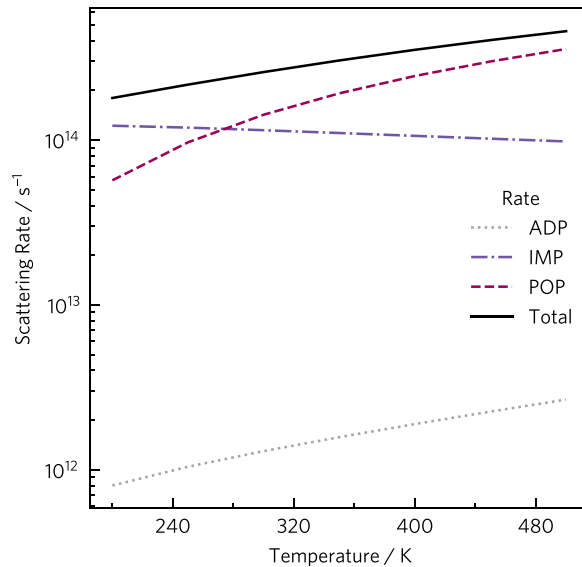
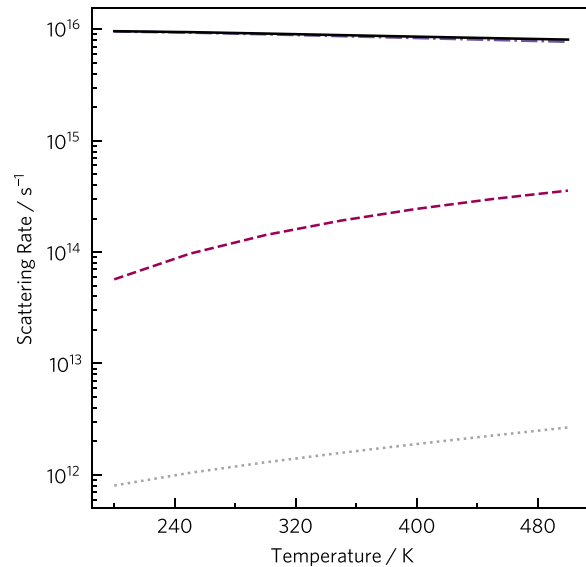
oxygen vacancy, which acts as a major charge compensating center. To boost the hole conductivity further, it is imperative that oxygen deficiency is minimized during growth, which could be achieved by using non-equilibrium growth techniques such as pulsed laser deposition (PLD) and molecular beam epitaxy (MBE).⁴² Unfortunately, these techniques do not scale well and are extraordinarily expensive, severely limiting the commercializability of p-type BaSnO₃ grown in this fashion.

The maximum hole concentration reported from experiment by Kim *et al.* is 1.0×10^{13} cm⁻³, falling within the predicted range and indeed suggesting room for around one order of magnitude improvement.⁸ From the present results, it is suggested that M^{XIII} doping, in particular In-doping, could generate an increased hole concentration that would improve the performance of a BaSnO₃ p-n homo-junction, reducing the mismatch between positive and negative carrier densities.

P-type charge transport properties were modeled using the AMSET package,³⁰ an extended explanation of which can be found in the supplementary material. Under the assumption of free-carrier transport, K-doping to a hole concentration of 5.2×10^{14} cm⁻³ will yield a maximum room temperature hole mobility of 5.96 cm² V⁻¹ s⁻¹, while In-doping to a hole concentration of 8.6×10^{15} cm⁻³ will

result in a 1.27 cm² V⁻¹ s⁻¹ mobility limit. Meanwhile, the mobilities reported for K-doped BaSnO₃ by Kim *et al.* range between 0.06 and 0.30 cm² V⁻¹ s⁻¹,⁸ in reasonably good agreement with the simulated value. Both theory and experiment suggest, therefore, that p-type BaSnO₃ will not display the high hole mobility required for p-type transparent conducting applications (critical for reaching high field-effect mobilities in p-n junctions), due to the highly localized VBM states. On the contrary, a hole mobility of 30 cm² V⁻¹ s⁻¹ has been measured in the p-type oxide Ba₂BiTaO₆ (which crystallizes in a rhombohedral “double-perovskite” structure) due to the strong interaction of Bi 6s² states with O 2p states at the VBM.^{43,44} This highlights valence band engineering as a strategy for increasing dispersion and thus hole mobility, shifting the focus away from pure oxides and toward light anion doping, such as N-doped BaSnO₃ (for which a hole mobility and carrier density of 0.86 cm² V⁻¹ s⁻¹ and 4.15×10^{16} cm⁻³ are reported, respectively),⁴⁵ formally mixed-anion systems,^{46–48} or even fully non-oxide materials.^{3,49–51}

Figure 5 shows the scattering rates that determine mobility at the maximum carrier concentrations for K- and In-doping. Considering first K-doping, at room temperature both ionized impurity scattering (IMP) and polar optical phonon (POP) scattering contribute significantly to the overall scattering rate [Fig. 5(a)]. The positive temperature dependence of POP scattering causes it to dominate at temperatures above 300 K, while the IMP rate remains fairly constant. The main contributing factor to the POP scattering at higher temperatures is the high-frequency O-dominated modes (as shown in the phonon density of states in the supplementary material, and as is typical in the n-type metal oxides),^{37,52} which could again be reduced by valence band engineering. Meanwhile, the increased number of charged defects that are present under In-doping (over 3 orders of magnitude compared to K-doping, as shown in Table II) result in a drastically

(a) K-doping (5.2×10^{14} cm⁻³)(b) In-doping (9.8×10^{15} cm⁻³)**FIG. 5.** Scattering rates against temperature for (a) K-doping and (b) In-doping. Acoustic deformation potential (ADP), ionized impurity (IMP), polar optical phonon (POP), and total scattering are in gray dots, lavender dash-dots, magenta dashes, and solid black, respectively. Plotted using ThermoParser.³¹

increased IMP scattering rate [Fig. 5(b)] that is responsible for the lower hole mobility of $1.27 \text{ cm}^2 \text{ V}^{-1} \text{ s}^{-1}$. These insights demonstrate the importance of not only dopability when searching for a p-type TCM but also the ability of a material to potentially withstand a high density of charged impurities.

It would seem that BaSnO_3 leans more toward tolerance than resistance of p-type doping compared to the other post-transition metal oxides: conductivity remains n-type in In_2O_3 even when doped with Mg to concentrations up to $6.0 \times 10^{20} \text{ cm}^{-3}$ due to over-compensation by oxygen vacancies;⁵³ p-type conduction can be achieved in SnO_2 when doped with N (between 1.5×10^{11} and $3.2 \times 10^{14} \text{ cm}^{-3}$ hole concentration), although no acceptor defects are predicted to enable performance higher than this;²⁵ ZnO can reportedly be doped to hole concentrations of 10^{18} cm^{-3} with N or Cu,^{54,55} although mobility is scarcely reported to exceed $1 \text{ cm}^2 \text{ V}^{-1} \text{ cm}^{-1}$,⁵⁶ while in Ga_2O_3 , Zn- or Fe-doping simply serves to reduce the n-type carrier concentration rather than inducing p-type carriers,⁵⁷ and DFT calculations suggest that p-type doping is infeasible.⁵⁸ This modest doping tolerance, combined with the fact that K-doping results in a relatively delocalized hole, rather than the highly localized anion-centered hole polarons that are exhibited in In_2O_3 , SnO_2 , and ZnO ,⁵⁹ suggest that p-type doping of BaSnO_3 is perhaps worth revisiting in the laboratory. The use of H as a co-dopant for lowering the formation energy of acceptor complexes, as seen in H:Mg-doped GaN,⁶⁰ might be a viable route for increasing the concentration of holes in BaSnO_3 and is certainly worth exploring. Similarly, light and heavy N-doping could also yield promising results, building on the initial experimental findings from Wang *et al.*⁴⁵

In summary, measurable p-type conductivity is predicted to be achievable in BaSnO_3 , but due to the inevitable presence of oxygen vacancy defects, it is unlikely to reach metallic-like levels, with hole densities capped at just under 10^{16} cm^{-3} . Of the group 1 metals Li, Na, and K, only the latter is predicted to be a reasonably good p-type dopant, with the former two undergoing self-compensation by low energy, n-type interstitial species. Meanwhile, all three group 13 metals examined should have low formation energies for p-type substitution, although they are significantly deeper and more polaronic in nature. K and In are the two species identified as most worthy of further experimental investigation, with In-doped BaSnO_3 being the most promising candidate for achieving maximum hole density within an all-perovskite, transparent p-n junction.

See the supplementary material for a full description of computational details, information pertaining to the AMSET calculations (calculated materials properties, explanation of scattering rates, compensation factors), phonon density of states, analysis of the oxygen vacancy, and tabulated limiting phases for the defect calculations.

J.W. acknowledges fruitful discussions with Dr Benjamin A. D. Williamson. J.W. and D.O.S. acknowledge Diamond Light Source Ltd for co-sponsorship of an EngD studentship on the EPSRC Centre for Doctoral Training in Molecular Modelling and Materials Science (No. EP/L015862/1). D.O.S. acknowledges support for EPSRC Grant No. EP/N01572X/1. This work used the ARCHER and ARCHER2 UK National Supercomputing Service (<https://www.archer2.ac.uk>), via our membership of the UK's HEC Materials Chemistry Consortium, which is funded by EPSRC (Nos. EP/

L000202, EP/R029431, and EP/T022213). We are grateful to the UK Materials and Molecular Modelling Hub for computational resources (Thomas and Young), which is partially funded by EPSRC (Nos. EP/P020194/1 and EP/T022213/1). The authors acknowledge the use of the UCL Myriad, Kathleen, and Thomas High Performance Computing Facilities (Myriad@UCL, Kathleen@UCL, Thomas@UCL), and associated support services, in the completion of this work.

AUTHOR DECLARATIONS

Conflict of Interest

The authors have no conflicts to disclose.

Author Contributions

Joe Willis: Conceptualization (equal); Data curation (lead); Formal analysis (lead); Investigation (lead); Methodology (equal); Software (equal); Validation (equal); Visualization (equal); Writing – original draft (lead); Writing – review & editing (equal). **Kieran B. Spooner:** Conceptualization (supporting); Data curation (supporting); Formal analysis (supporting); Investigation (supporting); Methodology (equal); Software (equal); Validation (equal); Visualization (equal); Writing – review & editing (equal). **David Oliver Scanlon:** Conceptualization (equal); Funding acquisition (lead); Project administration (lead); Resources (lead); Supervision (lead); Writing – review & editing (equal).

DATA AVAILABILITY

The data that support the findings of this study are available within the article and its supplementary material. The data that support the findings of this study are openly available at <https://doi.org/10.5281/zenodo.8325386>, Ref. 61.

REFERENCES

1. T. Minami, “Transparent conducting oxide semiconductors for transparent electrodes,” *Semicond. Sci. Technol.* **20**, S35–S44 (2005).
2. K. H. L. Zhang, K. Xi, M. G. Blamire, and R. G. Egdell, “P-type transparent conducting oxides,” *J. Phys.: Condens. Matter* **28**, 383002 (2016).
3. J. Willis and D. O. Scanlon, “Latest directions in p-type transparent conductor design,” *J. Mater. Chem. C* **9**, 11995–12009 (2021).
4. S. S. Shin, E. J. Yeom, W. S. Yang, S. Hur, M. G. Kim, J. Im, J. Seo, J. H. Noh, and S. I. Seok, “Colloidally prepared La-doped BaSnO_3 electrodes for efficient, photostable perovskite solar cells,” *Science* **356**, 167–171 (2017).
5. C. Granqvist and A. Hultåker, “Transparent and conducting ITO films: New developments and applications,” *Thin Solid Films* **411**, 1–5 (2002).
6. P. Barquinha, R. Martins, L. Pereira, and E. Fortunato, “A glance at current and upcoming applications,” in *Transparent Oxide Electronics: From Materials to Devices* (Wiley, 2012), pp. 267–286.
7. C. G. Granqvist, “Electrochromic oxide-based materials and devices for glazing in energy-efficient buildings,” in *Transparent Conductive Materials: Materials, Synthesis, Characterization, Application* (Wiley VCH, 2018), pp. 265–300.
8. H. M. Kim, U. Kim, C. Park, H. Kwon, and K. Char, “Thermally stable pn-junctions based on a single transparent perovskite semiconductor BaSnO_3 ,” *APL Mater.* **4**, 056105 (2016).
9. H. J. Kim, U. Kim, H. M. Kim, T. H. Kim, H. S. Mun, B.-G. Jeon, K. T. Hong, W.-J. Lee, C. Ju, K. H. Kim, and K. Char, “High mobility in a stable transparent perovskite oxide,” *Appl. Phys. Express* **5**, 061102 (2012).
10. S. Sallis, D. O. Scanlon, S. C. Chae, N. F. Quackenbush, D. A. Fischer, J. C. Woicik, J.-H. Guo, S. W. Cheong, and L. F. J. Piper, “La-doped

- BaSnO₃—Degenerate perovskite transparent conducting oxide: Evidence from synchrotron x-ray spectroscopy,” *Appl. Phys. Lett.* **103**, 042105 (2013).
- ¹¹C. A. Niedermeier, S. Rhode, K. Ide, H. Hiramatsu, H. Hosono, T. Kamiya, and M. A. Moram, “Electron effective mass and mobility limits in degenerate perovskite stannate BaSnO₃,” *Phys. Rev. B* **95**, 161202 (2017).
- ¹²S. Raghavan, T. Schumann, H. Kim, J. Y. Zhang, T. A. Cain, and S. Stemmer, “High-mobility BaSnO₃ grown by oxide molecular beam epitaxy,” *APL Mater.* **4**, 016106 (2016).
- ¹³D. O. Scanlon, “Defect engineering of BaSnO₃ for high-performance transparent conducting oxide applications,” *Phys. Rev. B* **87**, 161201 (2013).
- ¹⁴Z. Lebens-Higgins, D. O. Scanlon, H. Paik, S. Sallis, Y. Nie, M. Uchida, N. Quackenbush, M. Wahila, G. Sterbinsky, D. A. Arena, J. Woicik, D. G. Schlom, and L. F. J. Piper, “Direct observation of electrostatically driven band gap renormalization in a degenerate perovskite transparent conducting oxide,” *Phys. Rev. Lett.* **116**, 027602 (2016).
- ¹⁵L. Weston, L. Bjaalie, K. Krishnaswamy, and C. G. V. de Walle, “Origins of n-type doping difficulties in perovskite stannates,” *Phys. Rev. B* **97**, 054112 (2018).
- ¹⁶S. KC, A. J. E. Rowberg, L. Weston, and C. G. V. de Walle, “First-principles study of antisite defects in perovskite stannates,” *J. Appl. Phys.* **126**, 195701 (2019).
- ¹⁷H. Yabuta, N. Kaji, R. Hayashi, H. Kumomi, K. Nomura, T. Kamiya, M. Hirano, and H. Hosono, “Sputtering formation of p-type SnO thin-film transistors on glass toward oxide complimentary circuits,” *Appl. Phys. Lett.* **97**, 072111 (2010).
- ¹⁸G. Kresse and J. Hafner, “*Ab initio* molecular dynamics for liquid metals,” *Phys. Rev. B* **47**, 558–561 (1993).
- ¹⁹G. Kresse and J. Hafner, “*Ab initio* molecular-dynamics simulation of the liquid-metal-amorphous-semiconductor transition in germanium,” *Phys. Rev. B* **49**, 14251–14269 (1994).
- ²⁰G. Kresse and J. Hafner, “Norm-conserving and ultrasoft pseudopotentials for first-row and transition elements,” *J. Phys.: Condens. Matter* **6**, 8245–8257 (1994).
- ²¹G. Kresse and J. Furthmüller, “Efficiency of *ab-initio* total energy calculations for metals and semiconductors using a plane-wave basis set,” *Comput. Mater. Sci.* **6**, 15–50 (1996).
- ²²G. Kresse and J. Furthmüller, “Efficient iterative schemes for *ab initio* total-energy calculations using a plane-wave basis set,” *Phys. Rev. B* **54**, 11169–11186 (1996).
- ²³G. Kresse and D. Joubert, “From ultrasoft pseudopotentials to the projector augmented-wave method,” *Phys. Rev. B* **59**, 1758–1775 (1999).
- ²⁴C. Adamo and V. Barone, “Toward reliable density functional methods without adjustable parameters: The PBE0 model,” *J. Chem. Phys.* **110**, 6158–6170 (1999).
- ²⁵D. O. Scanlon and G. W. Watson, “On the possibility of p-type SnO₂,” *J. Mater. Chem.* **22**, 25236 (2012).
- ²⁶J. P. Perdew, A. Ruzsinszky, G. I. Csonka, O. A. Vydrov, G. E. Scuseria, L. A. Constantin, X. Zhou, and K. Burke, “Restoring the density-gradient expansion for exchange in solids and surfaces,” *Phys. Rev. Lett.* **100**, 136406 (2008).
- ²⁷W. Aggoune, A. Eljarrat, D. Nabok, K. Irmscher, M. Zupancic, Z. Galazka, M. Albrecht, C. Koch, and C. Draxl, “A consistent picture of excitations in cubic BaSnO₃ revealed by combining theory and experiment,” *Commun. Mater.* **3**, 12 (2022).
- ²⁸S. Lany and A. Zunger, “Assessment of correction methods for the band-gap problem and for finite-size effects in supercell defect calculations: Case studies for ZnO and GaAs,” *Phys. Rev. B* **78**, 235104 (2008).
- ²⁹S. Lany and A. Zunger, “Accurate prediction of defect properties in density functional supercell calculations,” *Modell. Simul. Mater. Sci. Eng.* **17**, 084002 (2009).
- ³⁰A. M. Ganose, J. Park, A. Faghaninia, R. Woods-Robinson, K. A. Persson, and A. Jain, “Efficient calculation of carrier scattering rates from first principles,” *Nat. Commun.* **12**, 2222 (2021).
- ³¹K. B. Spooner, M. Einhorn, D. W. Davies, and D. O. Scanlon, “ThermoParser: Streamlined analysis of thermoelectric properties” (2023), <https://github.com/SMTG-bham/ThermoParser>.
- ³²A. G. Squires, D. O. Scanlon, and B. J. Morgan, “py-sc-fermi: Self-consistent fermi energies and defect concentrations from electronic structure calculations,” *J. Open Source Software* **8**, 4962 (2023).
- ³³J. Buckeridge, “Equilibrium point defect and charge carrier concentrations in a material determined through calculation of the self-consistent fermi energy,” *Comput. Phys. Commun.* **244**, 329–342 (2019).
- ³⁴J. Buckeridge, D. Scanlon, A. Walsh, and C. Catlow, “Automated procedure to determine the thermodynamic stability of a material and the range of chemical potentials necessary for its formation relative to competing phases and compounds,” *Comput. Phys. Commun.* **185**, 330–338 (2014).
- ³⁵K. Momma and F. Izumi, “VESTA 3 for three-dimensional visualization of crystal, volumetric and morphology data,” *J. Appl. Crystallogr.* **44**, 1272–1276 (2011).
- ³⁶A. M. Ganose, A. J. Jackson, and D. O. Scanlon, “sumo: Command-line tools for plotting and analysis of periodic *ab initio* calculations,” *J. Open Source Software* **3**, 717 (2018).
- ³⁷K. B. Spooner, A. G. Ganose, and D. O. Scanlon, “Assessing the limitations of transparent conducting oxides as thermoelectrics,” *J. Mater. Chem. A* **8**, 11948 (2020).
- ³⁸V. M. Goldschmidt, “Die Gesetze der Kristallochemie,” *Naturwissenschaften* **14**, 477–485 (1926).
- ³⁹R. D. Shannon, “Revised effective ionic radii and systematic studies of interatomic distances in halides and chalcogenides,” *Acta Crystallogr., Sect. A* **32**, 751–767 (1976).
- ⁴⁰I. Mosquera-Lois, S. R. Kavanagh, A. Walsh, and D. O. Scanlon, “ShakeNBreak: Navigating the defect configurational landscape,” *J. Open Source Software* **7**, 4817 (2022).
- ⁴¹I. Mosquera-Lois, S. R. Kavanagh, A. Walsh, and D. O. Scanlon, “Identifying the ground state structures of point defects in solids,” *npj Comput. Mater.* **9**, 25 (2023).
- ⁴²S. C. Dixon, S. Sathasivam, B. A. D. Williamson, D. O. Scanlon, C. J. Carmalt, and I. P. Parkin, “Transparent conducting n-type ZnO:Sc—Synthesis, optoelectronic properties and theoretical insight,” *J. Mater. Chem. C* **5**, 7585–7597 (2017).
- ⁴³A. Bhatia, G. Hautier, T. Nilgianskul, A. Miglio, J. Sun, H. J. Kim, K. H. Kim, S. Chen, G.-M. Rignanese, X. Gonze, and J. Suntivich, “High-mobility bismuth-based transparent p-type oxide from high-throughput material screening,” *Chem. Mater.* **28**, 30–34 (2016).
- ⁴⁴J. Shi, E. A. Rubinstein, W. Li, J. Zhang, Y. Yang, T.-L. Lee, C. Qin, P. Yan, J. L. MacManus-Driscoll, D. O. Scanlon, and K. H. Zhang, “Modulation of the Bi³⁺ 6s² lone pair state in perovskites for high-mobility p-type oxide semiconductors,” *Adv. Sci.* **9**, 2104141 (2022).
- ⁴⁵J. Wang and B. Luo, “Electronic properties of p-type BaSnO₃ thin films,” *Ceram. Int.* **46**, 25678–25682 (2020).
- ⁴⁶M. Einhorn, B. A. D. Williamson, and D. O. Scanlon, “Computational prediction of the thermoelectric performance of LaZnOPn (Pn = P, As),” *J. Mater. Chem. A* **8**, 7914–7924 (2020).
- ⁴⁷K. Brlec, K. B. Spooner, J. M. Skelton, and D. O. Scanlon, “Y₂Ti₂O₅S₂—A promising n-type oxysulphide for thermoelectric applications,” *J. Mater. Chem. A* **10**, 16813–16824 (2022).
- ⁴⁸K. Brlec, C. N. Savory, and D. O. Scanlon, “Understanding the electronic structure of Y₂Ti₂O₅S₂ for green hydrogen production: A hybrid-DFT and GW study,” *J. Mater. Chem. A* **11**, 16776–16787 (2023).
- ⁴⁹B. A. D. Williamson, J. Buckeridge, J. Brown, S. Ansbro, R. G. Palgrave, and D. O. Scanlon, “Engineering valence band dispersion for high mobility p-type semiconductors,” *Chem. Mater.* **29**, 2402–2413 (2017).
- ⁵⁰J. Willis, I. Bravić, R. R. Schnepf, K. N. Heinselman, B. Monserrat, T. Unold, A. Zakutayev, D. O. Scanlon, and A. Crovetto, “Prediction and realisation of high mobility and degenerate p-type conductivity in CaCuP thin films,” *Chem. Sci.* **13**, 5872–5883 (2022).
- ⁵¹J. Willis, R. Claes, Q. Zhou, M. Giantomassi, G.-M. Rignanese, G. Hautier, and D. O. Scanlon, “Limits to hole mobility and doping in copper iodide,” [10.26344/chemrxiv-2023-lttnf](https://arxiv.org/abs/2023.10.26344) (2023).
- ⁵²K. B. Spooner, A. M. Ganose, W. W. Leung, J. Buckeridge, B. A. Williamson, R. G. Palgrave, and D. O. Scanlon, “BaBi₂O₆: A promising n-type thermoelectric oxide with the PbSb₂O₆ crystal structure,” *Chem. Mater.* **33**, 7441 (2021).
- ⁵³O. Bierwagen and J. S. Speck, “Mg acceptor doping of In₂O₃ and overcompensation by oxygen vacancies,” *Appl. Phys. Lett.* **101**, 102107 (2012).
- ⁵⁴J. M. Bian, X. M. Li, C. Y. Zhang, W. D. Yu, and X. D. Gao, “p-type ZnO films by monodoping of nitrogen and ZnO-based p-n homojunctions,” *Appl. Phys. Lett.* **85**, 4070–4072 (2004).

- ⁵⁵M. Suja, S. B. Bashar, M. M. Morshed, and J. Liu, "Realization of Cu-doped p-type ZnO thin films by molecular beam epitaxy," *ACS Appl. Mater. Interfaces* **7**, 8894–8899 (2015).
- ⁵⁶J. Fan, K. Sreekanth, Z. Xie, S. Chang, and K. Rao, "P-type ZnO materials: Theory, growth, properties and devices," *Prog. Mater. Sci.* **58**, 874–985 (2013).
- ⁵⁷Y. Ueda, T. Igarashi, K. Koshi, S. Yamakoshi, K. Sasaki, and A. Kuramata, "Two-inch Fe-doped Ga₂O₃ (010) substrates prepared using vertical Bridgman method," *Jpn. J. Appl. Phys., Part 1* **62**, SF1006 (2023).
- ⁵⁸A. Kyrtos, M. Matsubara, and E. Bellotti, "On the feasibility of p-type Ga₂O₃," *Appl. Phys. Lett.* **112**, 032108 (2018).
- ⁵⁹S. Lany and A. Zunger, "Polaronic hole localization and multiple hole binding of acceptors in oxide wide-gap semiconductors," *Phys. Rev. B* **80**, 085202 (2009).
- ⁶⁰J. Neugebauer and C. G. V. de Walle, "Hydrogen in GaN: Novel aspects of a common impurity," *Phys. Rev. Lett.* **75**, 4452–4455 (1995).
- ⁶¹J. Willis (2023). "On the possibility of p-type doping in barium stannate," Zenodo. <https://doi.org/10.5281/zenodo.8325386>